Pergamon

Int. J. Heat Mass Transfer. Vol. 39, No. 1, pp. 135–147, 1996
Copyright © 1995 Elsevier Science Ltd
Printed in Great Britain. All rights reserved
0017–9310/96 $9.50+0.00

0017–9310(95)00093–3

Heat transfer enhancement in water–feldspar upflows through vertical annuli

TÜLAY A. ÖZBELGE and SEMA H. KÖKER

Department of Chemical Engineering, Middle East Technical University, Ankara 06531, Turkey

(*Received* 7 *June* 1994 *and in final form* 9 *February* 1995)

Abstract—Although there are many industrial applications of liquid–solid flows in technology, the available knowledge of heat transfer to or from such flows is limited. In this study the effects of parameters on the enhancement of heat transfer from water–feldspar slurries flowing turbulently upwards in vertical annuli were investigated and the experimental conditions beneficial to the enhancement of heat transfer were determined. It was found that the heat transfer enhancement in upflow of slurries through a vertical annulus was a function of Prandtl and flow Reynolds numbers, the ratio of equivalent diameter to particle diameter, the aspect ratio of the inner pipe diameter to the outer pipe diameter and the concentration of solid particles in the slurry.

INTRODUCTION

The subject of heat transfer in particulate flows became popular during the 1950s, when seeding the flow with micrometre-size solid particles was considered as a "heat transfer augmentation technique" [1, 2].

Enhancement or augmentation of heat transfer by introduction of solids into fluids offered many advantages to conventional cooling of nuclear reactors [1]. Since the same heat transfer rates could be achieved at lower system pressures, costs were reduced due to the smaller heat transfer area requirement and the lower cost of construction materials at the reduced pressures. The same technique was used to overcome the deficiencies of gases and liquids in using them as heat transfer media [3].

The heat transfer and flow characteristics of liquid–solid flows in horizontal and vertical pipes were investigated by several researchers [3–10]; however, liquid–solid and gas–solid flows in annuli were not studied adequately due to their complicated nature.

The relationship between the heat transfer enhancement due to the presence of solid particles and the fluid–solid interactions in horizontal and vertical pipe flows of suspensions was studied by several researchers; relatively recent investigations were made by Brandon and Thomas [5], Plass and Molerus [6] and Zisselmar and Molerus [11]. In all these studies, it was proved that in the viscous sublayer the strong mutual interaction between the fluid and solid phases increased the turbulent intensity, thus the solid particles enhanced the wall-to-suspension heat transfer by thinning the viscous sublayer. Brandon and Thomas [5] obtained a dimensionless grouping, $d_p^* = (d_p/D)(Re)^{11/16}$ and reported the occurrence of a peak heat transfer enhancement at a constant value of d_p^* which was found to be 4.4 for water–glass powder suspension flows. Özbelge [8] investigated the applicability of the model proposed by Brandon and Thomas [5] and concluded that a particular combination of particle size, pipe diameter, flow Reynolds number and solid concentration would determine the magnitude of the peak heat transfer enhancement in suspension flows, while its location was set by d_p^* in accordance with the interaction model [5]. Özbelge [8] further reported d_p^* as 4.2 for water–feldspar slurries flowing turbulently in horizontal pipes. This model has not yet been checked for liquid–solid flows in annuli and more research is needed to clarify the two-phase heat transfer mechanism in a vertical annulus. The objective of the present study is to provide experimental data to be used in the design and modelling work.

EXPERIMENTAL

In the experimental investigation of heat transfer to or from liquid–solid flows in a vertical annulus, the chosen independent variables are particle size, solid concentration, flow Reynolds number and the aspect ratio, which is the ratio of the outside diameter of the inner pipe to the inside diameter of the outer pipe. The convective heat transfer coefficients, heat transfer enhancement ratio and the Nusselt numbers of suspension flows in the annulus have been determined.

Experimental set-up

The apparatus used in the experiments is shown in Fig. 1. It consists of two main lines, a hot slurry line and a cold water line. The slurry line forms a closed loop system which has the following items: a slurry pump, and a heat exchanger on the horizontal line to heat the slurry to the desired temperature with steam before entering the vertical annulus of 4.1 m in length.

NOMENCLATURE

A_f flow area of annulus [m^2]
A_{ii} tube-side heat transfer area, $\pi D_{ii} L$ [m^2]
A_{io} annulus-side heat transfer area, $\pi D_{io} L$ [m^2]
C heat capacity [J kg^{-1} K^{-1}]
C_f solid concentration in the feed slurry [wt%]
D pipe diameter [mm]
D_e equivalent diameter of annulus [mm]
d_p^* dimensionless grouping, $(d_p/D)(Re)^{11/16}$
d_p particle diameter [mm or μm]
D_{ii} inside diameter of inner pipe [mm]
D_{io} outside diameter of inner pipe [mm]
D_{oi} inside diameter of outer pipe [mm]
h heat transfer coefficient [W m^{-2} K^{-1}]
k thermal conductivity [W m^{-1} K^{-1}]
k_{Cu} thermal conductivity of copper tube [W m^{-1} K^{-1}]
L length of test section [m]
$\dot{m}$ mass flow rate [kg s^{-1}]
Nu Nusselt number
Pr Prandtl number
q heat transfer rate [W]
q_{Loss} rate of heat loss to surroundings [W]
Re Reynolds number
T temperature [°C]
u velocity [m s^{-1} or cm s^{-1}]
U_o overall heat transfer coefficient
X weight fraction of solids in slurry [kg kg^{-1}].

Greek symbols
ΔT_{LM} logarithmic temperature difference [K]
κ aspect ratio, D_{io}/D_{oi}
μ viscosity [kg m^{-1} s^{-1}]
ρ density [kg m^{-3}]
Φ volume fraction of solids in suspension.

Subscripts
p solid particle
s suspension or slurry
si slurry inlet
so slurry outlet
sw water in annulus side
w water in tube side
wi cooling water inlet to tube side
wo cooling water outlet.

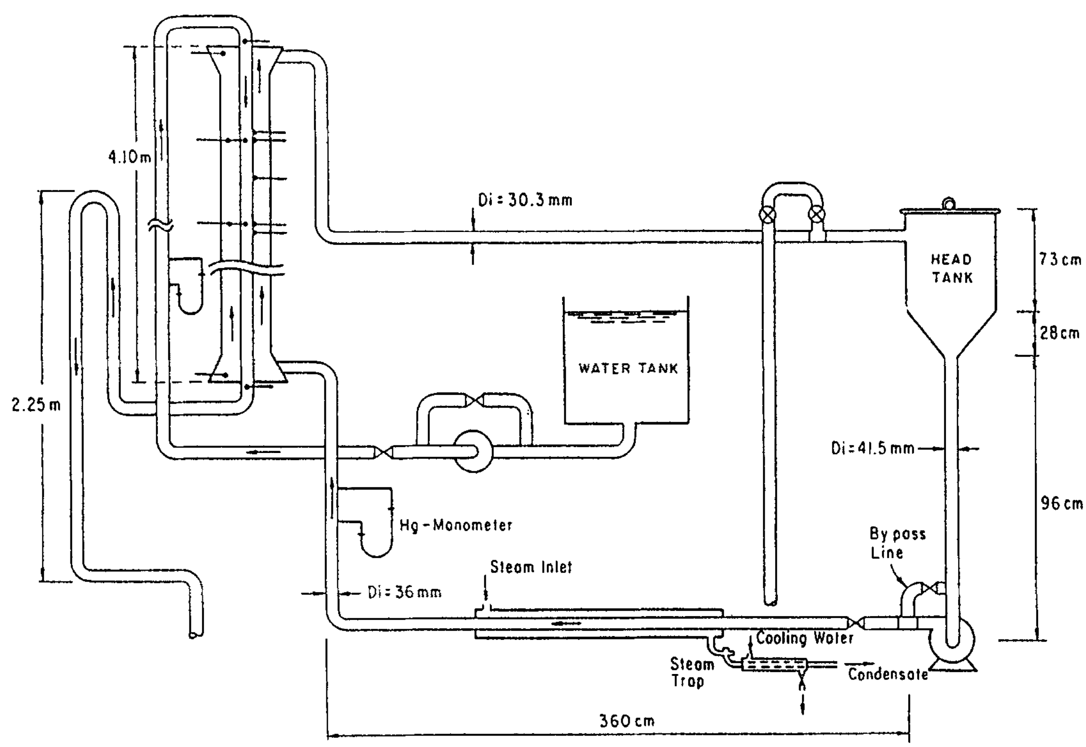

Fig. 1. Schematic of the experimental set-up.

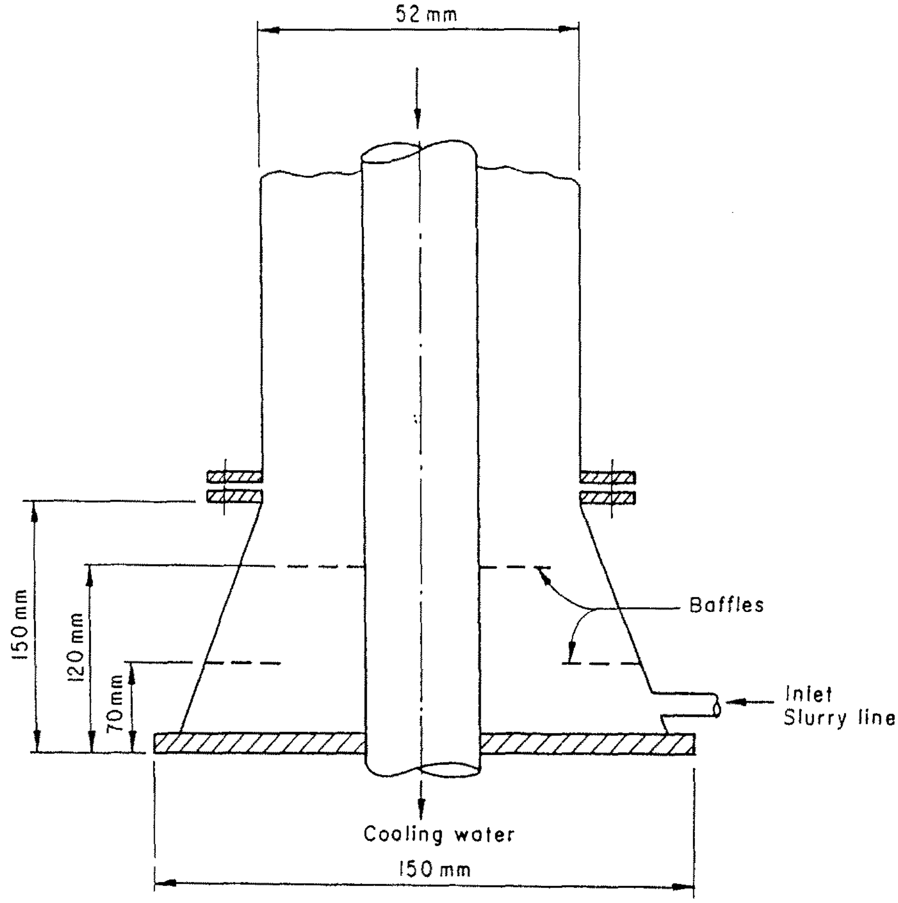

Fig. 2. A schematic diagram of the flared mixing chamber.

The vertical test section is the 1.22 m section of the annulus. An entrance length of 1.57 m was provided from the bottom end of the annulus to the test section to ensure fully developed velocity and temperature profiles in the test section. The annulus has flared mixing chambers at both its ends, equipped with baffles to provide uniform flow of liquid–solid mixtures. A schematic diagram of the flared section is shown in Fig. 2.

The cold-water line consists of a constant-level tank with an overflow line to the drain and a centrifugal pump which forces the cooling water upwards in a vertical pipeline to the top of the annulus, then it flows downwards through the inner pipe of the annulus and again upwards in a hydraulic leg approximately 2 m long at the end of the annulus to prevent leakage of air into the system.

The slurry and cooling water flow rates were measured with previously calibrated orifice meters placed on the corresponding lines away from the elbows to avoid flow disturbances. Shielded iron–constantan thermocouples used to measure slurry temperatures extended into the annulus horizontally with their tips in-between the inner and outer pipes, while the thermocouples measuring water temperatures extended into the centre of the inner pipe. Utmost care was provided to avoid leakage between the annulus and the inner pipe, and to minimize the flow disturbance in the test section. Shielded iron–constantan thermocouples of surface type were used to measure the wall temperatures on the outside surface of the inner pipe and they were fixed by bolts-and-nuts arrangements on the outside surface of the outer pipe.

The solid particles used in heat transfer experiments were feldspar with the physical properties given in Table 1. Three batches of particles with different average diameters were prepared by using a series of Tyler standard sieves. Arithmetic average diameters between the sieves were taken as the average diameter for each batch of particles. In the experiments three concentric pipe-sets were used. The details for these pipe-sets are given in Table 2.

Experimental procedure

At the start of this work, the orifice meters were calibrated. The thermocouple calibrations were checked by using a temperature-controlled water bath and a thermometer accurate to $\pm 0.05^{\circ}C$. This procedure was repeated at the beginning of experiments with each concentric pipe-set, then the thermocouples were placed into their positions carefully, and the system was insulated with fibre glass. The accuracy and

Table 1. Physical properties of solids

Material	ρ_p [kg m^{-3}]	d_p [mm]	C_p [J kg^{-1} K^{-1}]	k_p [W m^{-1} K^{-1}]
Feldspar ($K_2O \cdot Al_2O_3 \cdot SiO_2$)	2500	0.072 0.127 0.191	836.8	1.09

Table 2. Characteristics of concentric pipe-sets

Pipe-set	Material of construction	D_{oi} [mm]	D_{io} [mm]	κ	A_f [m^2]	D_e [mm]
I	Outer pipe: galvanized iron Inner pipe: copper	52	16	0.308	1.923×10^{-3}	36
II	Outer pipe: galvanized iron Inner pipe: copper	52	22	0.423	1.744×10^{-3}	30
III	Outer pipe: galvanized iron Inner pipe: copper	52	28	0.538	1.508×10^{-3}	24

the reproducibility of the results were tested in several runs with water only. The hot water flowing upwards in the annulus was cooled by cold water countercurrently. Thus, the heat transfer coefficients of a single phase, namely of water in the annulus, were determined according to the calculation procedure given in this paper, and they were compared with the heat transfer correlation given by Petukhov and Roizen [12]. In addition to this, some of the runs were repeated at almost the same operating conditions to check the reproducibility. Afterwards, the experiments with solid particles in water were started. The scope of these experiments are given in Table 3. The general experimental procedure consisted of the following steps.

(1) The slurry side of the system was filled with water and the pump was started. The slurry of required concentration with a uniform particle size was prepared by dumping the necessary amount of solids into the head tank, since the volume of the system and the density of solids were measured previously. The liquid level in the head tank was checked to be at the marked level.

(2) The flow rates of the slurry and the cooling water were set at the desired values.

(3) The slurry was heated with steam to a temperature within a range of 40–65°C in the horizontal heat exchanger, then it entered the vertical annulus from the bottom. At each aspect ratio, and each slurry velocity, the flow rate of the cooling water was so adjusted that a reasonable temperature difference for each stream was obtained between the inlet and the outlet of the test section. Thus, the experimental error in the thermocouple measurements was minimized and an almost linear temperature variation in each stream along the overall length of the vertical annulus was provided.

(4) Actual data were recorded within 10 min after the system reached the steady state, which required approximately an hour or more. At the steady state, slurry and cooling water temperatures at the inlet and outlet of the overall length of the vertical annulus and of the test section, the wall temperatures and the pressure differentials of the orifice meters were recorded.

(5) Transport concentration of solids in the flowing slurry was determined with a gravimetric technique after obtaining a sample of slurry from the sampling line on the annulus when the steady state was reached in each run. Further details of the experimental work are given elsewhere [13].

(6) At the end of the day of experimentation, the solids were washed out of the system and the pumps were turned off.

Calculation procedure

The heat flow rate from the hot slurry to the cold water in the test section is given by the following equation:

$$q_s = \dot{m}_s C_s (T_{si} - T_{so}). \quad (1)$$

Table 3. Scope of the heat transfer experiments

Feed slurry concentration, C_f [wt%]	0.75	$< C_f$	< 2.5
Solid particle size, d_p [mm]	0.072	$< d_p$	< 0.191
Slurry Reynolds number, Re_s	15 500	$< Re_s$	$< 55\,500$
Slurry velocity in annulus, u_s [m s^{-1}]	0.248	$< u_s$	< 1.25
Aspect ratio, κ	0.308	$< \kappa$	< 0.538

The rate of heat transfer to the cooling water in the test section is equal to:

$$q_w = \dot{m}_w C_w (T_{wo} - T_{wi}). \quad (2)$$

The net rate of heat transfer through the wall to the cooling water can be calculated as follows:

$$q_s - q_{Loss} = q_w = U_o A_{io} \Delta T_{LM} \quad (3)$$

where

$$U_o A_{io} = \left\{ \frac{1}{h_w \pi D_{ii} L} + \frac{\ln(D_{io}/D_{ii})}{2\pi L k_{Cu}} + \frac{1}{h_s \pi D_{io} L} \right\}^{-1} \quad (4)$$

and

$$\Delta T_{LM} = \frac{(T_{si} - T_{wo}) - (T_{so} - T_{wi})}{\ln\{(T_{si} - T_{wo})/(T_{so} - T_{wi})\}} \quad (5)$$

$$A_{io} = \pi D_{io} L. \quad (6)$$

For the calculation of tube-side heat transfer coefficient for the cooling water, h_w, Sieder and Tate's equation [14] was used:

$$(h_w D_{ii}/k_w) = 0.023(D_{ii} u_w \rho_w/\mu_w)^{0.8} \times (C_w \mu_w/k_w)^{1/3} (\mu_w/\mu_{wall})^{0.14} \quad (7)$$

where the physical properties of water were calculated at the bulk mean temperature of the cooling water in the tube side of the test section. The individual heat transfer coefficients of liquid–solid flows, h_s, were calculated using equations (2)–(7).

The physical properties of dilute liquid–solid suspensions at the bulk mean annular-side temperatures were obtained by the modifications of water properties for the presence of solids according to their concentrations. The volume-averaged density and the weight-averaged heat capacity were calculated from the following equations:

$$\rho_s = \rho_{sw}(1-\Phi) + \rho_p \Phi \quad (8)$$

$$C_s = C_{sw}(1-X) + C_p X \quad (9)$$

where X and Φ are the mass and the volume fractions of the solids in the suspension, respectively.

The following equations recommended in the literature [3, 15] were used for the calculation of the suspension viscosity and thermal conductivity, respectively:

$$\mu_s = \mu_{sw}(1 + 2.5\Phi + 7.17\Phi^2 + 16.2\Phi^3) \quad (10)$$

$$k_s = k_{sw}\left(\frac{2k_{sw} + k_p - 2\Phi(k_{sw} - k_p)}{2k_{sw} + k_p + \Phi(k_{sw} - k_p)}\right). \quad (11)$$

For the thermal conductivity of the copper tube, k_{Cu}, a value of 379 W m^{-1}°C^{-1} was used [13]. The dimensionless numbers for liquid–solid flows in the annulus were defined as follows:

$$Nu_s = h_s D_e/k_s \quad Pr_s = C_s \mu_s/k_s \quad Re_s = D_e u_s \rho_s/\mu_s. \quad (12)$$

RESULTS AND DISCUSSION

Several experiments were performed with hot-water flow without solids in the annulus cooled by cold-water flow in the tube side to check the accuracy of the experimental system. The experimental Nusselt numbers for the water flow in the annulus were calculated using equations (2)–(7) and (14). The theoretical Nusselt number, Nu_{sw}, for each experiment was also calculated from the correlation by Petukhov and Roizen [12], which is given for a single-phase annular flow as follows:

$$Nu_{sw} = \frac{(f/8)(Re_{sw} - 1000)Pr_{sw}(0.86)\kappa^{-0.16}}{(1 + 12.7(\sqrt{f/8})(Pr_{sw}^{2/3} - 1))} \quad (13)$$

where

$$Nu_{sw} = h_{sw} D_e/k_{sw} \quad Pr_{sw} = C_{sw} \mu_{sw}/k_{sw}$$

$$Re_{sw} = D_e u_{sw} \rho_{sw}/\mu_{sw} \quad (14)$$

$$f = (1.82 \log_{10} Re_{sw} - 1.64)^{-2}. \quad (15)$$

The subscript sw was used for water flow in the annulus without solids; Re_{sw} and Pr_{sw} were calculated using the properties of water at the bulk-mean water temperature in the annulus. It was observed that the discrepancies between the experimental Nu_{sw} values and those from the correlation [12] were less than 9%. This cumulative error included the inaccuracies due to the use of Sieder and Tate's [14] correlation to calculate the tube-side heat transfer coefficients, the possible experimental errors such as heat loss, temperature and flow rate measurements and the inaccuracy of the Petukhov and Roizen [12] correlation. The heat loss was around 1%. The effect of entrance length was not important since the L/D_e ratio was changed between 78 and 116 in the range of experiments. The reproducibility of the repeated runs performed with the slurry flow in the annulus was around 10%. Considering the experimental difficulties experienced with the particulate flows, these results should be acceptable.

The individual heat transfer coefficients of liquid–solid flows, h_s, at different operating conditions calculated from the experimental data given in Table 4 using equations (2)–(7) were plotted with respect to the slurry Reynolds numbers for each particle size and for each aspect ratio, taking the solid concentration as a parameter (Figs. 3–11). The individual heat transfer coefficients for water flow in the annulus, h_{sw}, calculated from equations (13)–(15), were also plotted with respect to the Re_{sw} values in Figs. 3–11 and a straight line for each aspect ratio (κ) was obtained to be used as a reference for the determination of enhancement in the slurry heat transfer coefficient, if any, by the addition of solid particles to water. It has to be noted that the ranges of the Reynolds and Prandtl numbers in the experiments performed in the annuli with different aspect ratios were not the same,

Table 4. Experimental data and calculated results

C_f [wt%]	$\dot{m}_w$ [kg s^{-1}]	$\dot{m}_s$ [kg s^{-1}]	T_{si} [°C]	T_{so} [°C]	T_{wi} [°C]	T_{wo} [°C]	Re_w	Pr_w	h_w [W m^{-2} K^{-1}]	Re_s	Pr_s	Nu_s	h_s [W m^{-2}K^{-1}]	h_s/h_{sw}
$d_p = 72$ μm, $\kappa = 0.308$, $D_e = 36$ mm, $A_{ii} = \pi(0.014)(1.22)$ m^2, $A_{io} = \pi(0.016)(1.22)$ m^2														
0.75	0.396	0.6310	59.20	57.60	24.55	27.05	40 914	6.06	9668	24 430	3.08	152	2765	1.17
0.75	0.396	0.9914	57.10	55.90	25.55	28.45	42 049	5.87	9744	36 978	3.21	216	3901	1.12
0.75	0.385	1.1234	57.15	55.95	26.00	29.30	41 481	5.78	9588	41 917	3.21	262	4732	1.23
0.75	0.385	1.4975	55.60	54.65	26.50	30.05	42 174	5.67	9623	54 580	3.29	325	5863	1.30
1.25	0.398	0.6310	58.90	57.20	23.50	26.10	40 129	6.23	9602	24 019	3.12	192	3492	1.48
1.25	0.398	0.9914	56.80	55.50	24.40	27.50	41 213	6.04	9674	36 650	3.22	233	4216	1.21
1.25	0.385	1.1234	57.25	56.05	25.20	28.55	40 816	5.89	9524	41 835	3.20	256	4641	1.21
1.25	0.385	1.4975	55.65	54.70	26.40	29.90	41 873	5.72	9601	54 426	3.28	322	5817	1.27
2.50	0.396	0.6310	58.90	57.30	23.30	25.75	39 664	6.28	9548	23 742	3.12	143	2599	1.11
2.50	0.396	0.9914	57.15	55.95	25.40	28.30	41 906	5.89	9737	36 424	3.20	213	3864	1.14
2.50	0.385	1.1234	57.25	56.10	26.10	29.25	41 774	5.73	9625	41 224	3.20	241	4369	1.16
2.50	0.385	1.4975	53.75	52.85	26.45	29.75	41 824	5.72	9558	52 138	3.39	329	5946	1.34
$d_p = 127$ μm, $\kappa = 0.308$, $D_e = 36$ mm, $A_{ii} = \pi(0.014)(1.22)$ m^2, $A_{io} = \pi(0.016)(1.22)$ m^2														
0.75	0.395	0.6310	58.15	56.45	23.70	26.20	39 902	6.21	9530	23 846	3.17	155	2797	1.18
0.75	0.395	0.9830	56.65	55.50	31.55	27.35	40 895	6.04	9613	36 837	3.20	195	3516	1.00
0.75	0.370	1.1234	56.85	55.70	25.50	28.85	39 449	5.85	9244	42 034	3.19	254	4595	1.20
0.75	0.370	1.4975	55.40	54.45	26.20	29.95	40 207	5.72	9294	54 551	3.29	351	6340	1.38
1.25	0.398	0.6310	58.80	57.00	23.90	26.65	40 618	6.14	9658	23 972	3.13	175	3167	1.33
1.25	0.398	0.9914	56.85	55.55	25.30	28.45	42 117	5.89	9762	36 434	3.24	248	4485	1.28
1.25	0.385	1.1234	56.45	55.25	24.90	28.30	40 584	5.93	9487	41 358	3.23	270	4897	1.25
1.25	0.385	1.4975	54.50	53.50	25.10	28.90	40 908	5.87	9483	53 416	3.35	377	6801	1.49
2.50	0.398	0.6310	56.70	55.35	24.80	26.80	41 074	6.06	9663	22 933	3.23	126	2297	1.00
2.50	0.396	0.9914	56.70	55.40	25.65	28.65	42 345	5.83	9758	36 506	3.22	233	4227	1.22
2.50	0.385	1.1234	56.95	55.75	26.35	29.65	41 775	5.72	9623	41 083	3.21	268	4868	1.25
2.50	0.385	1.4975	54.10	53.15	26.50	29.85	41 924	5.71	9573	52 751	3.36	331	5992	1.32
$d_p = 191$ μm, $\kappa = 0.308$, $D_e = 36$ mm, $A_{ii} = \pi(0.014)(1.22)$ m^2, $A_{io} = \pi(0.016)(1.22)$ m^2														
0.75	0.396	0.6230	61.70	59.90	25.50	28.05	41 857	5.91	9807	24 857	2.97	147	2670	1.11
0.75	0.390	0.9914	58.40	57.20	25.20	28.10	41 113	5.92	9616	37 611	3.16	196	3547	1.00
0.75	0.363	1.1234	58.20	56.95	25.55	29.30	39 584	5.82	9293	42 338	3.18	274	4955	1.27
0.75	0.350	1.4975	57.20	56.20	27.20	31.40	38 763	5.59	8988	55 624	3.22	401	7245	1.57
1.25	0.396	0.6310	56.80	55.20	24.00	26.35	40 463	6.14	9567	23 336	3.22	152	2753	1.23
1.25	0.398	0.9914	54.85	53.80	25.60	28.10	42 068	5.89	9724	35 560	3.33	195	3517	1.05
1.25	0.385	1.1234	56.45	55.40	26.40	29.35	41 679	5.76	9579	41 273	3.24	231	4177	1.11
1.25	0.385	1.4975	54.90	53.90	26.55	30.15	42 071	5.69	9602	53 712	3.33	361	6514	1.44
2.50	0.396	0.6470	53.70	52.20	24.50	26.80	40 917	6.07	9555	22 434	3.40	175	3155	1.45
2.50	0.398	0.9914	52.80	51.75	25.15	27.65	41 541	5.98	9627	34 024	3.44	213	3852	1.17
2.50	0.385	1.1234	53.95	52.90	26.00	28.90	41 290	5.82	9493	39 432	3.36	254	4594	1.25
2.50	0.385	1.4975	54.40	53.50	26.90	30.15	42 172	5.67	9607	52 945	3.35	315	5683	1.26

$d_p = 72\ \mu m$, $\kappa = 0.423$, $D_e = 30$ mm, $A_{ii} = \pi(0.020)(1.22)\ m^2$, $A_{io} = \pi(0.022)(1.22)\ m^2$														
0.75	0.436	0.6310	55.90	54.00	23.20	25.75	30 538	6.29	5380	21 208	3.29	138	2992	1.23
0.75	0.432	0.9914	54.80	53.55	23.85	26.55	30 757	6.17	5363	32 738	3.34	160	3470	1.00
0.75	0.428	1.1176	54.55	53.50	24.95	27.65	31 325	5.98	5391	36 831	3.35	204	4414	1.00
0.75	0.407	1.4880	54.20	53.30	25.70	28.95	30 478	5.83	5218	48 836	3.36	245	5298	1.10
1.25	0.427	0.6310	55.65	54.00	23.65	25.95	30 133	6.23	5313	21 041	3.28	113	2461	1.04
1.25	0.427	0.9914	54.50	53.20	24.35	27.20	30 900	6.06	5359	32 368	3.36	180	3893	1.06
1.25	0.407	1.1234	54.30	53.20	25.25	28.10	30 060	5.92	5196	36 676	3.36	181	3907	1.00
1.25	0.390	1.4975	51.05	50.20	24.25	27.40	28 205	6.06	4949	46 677	3.54	256	5507	1.18
2.50	0.426	0.6390	56.95	55.20	24.40	26.90	30 674	6.09	5358	21 412	3.22	125	2720	1.11
2.50	0.432	0.9914	55.15	53.90	25.15	27.90	31 802	5.94	5454	34 043	3.15	170	3697	1.00
2.50	0.393	1.4975	53.20	52.30	26.05	29.25	29 618	5.79	5089	47 516	3.42	252	5462	1.14
$d_p = 127\ \mu m$, $\kappa = 0.423$, $D_e = 30$ mm, $A_{ii} = \pi(0.020)(1.22)\ m^2$, $A_{io} = \pi(0.022)(1.22)\ m^2$														
0.75	0.428	0.9630	54.25	53.05	23.80	26.35	30 410	6.19	5324	31 561	3.37	146	3142	1.01
0.75	0.413	1.1119	54.25	53.10	23.70	26.65	29 419	6.17	5171	36 458	3.37	181	3908	1.00
0.75	0.413	1.4975	52.25	51.40	24.15	27.15	29 749	6.09	5176	47 796	3.47	221	4754	1.00
0.75	0.432	0.6310	56.60	54.90	24.30	26.65	30 962	6.12	5408	21 316	3.24	117	2533	1.05
1.25	0.436	0.9830	54.65	53.40	24.75	27.40	31 715	6.02	5457	32 254	3.34	163	3532	1.00
1.25	0.405	1.1234	54.05	52.85	23.65	26.80	28 871	6.16	5093	36 524	3.38	204	4408	1.12
1.25	0.393	1.4975	53.45	52.50	24.45	27.85	28 658	6.01	5012	48 344	3.40	254	5488	1.15
1.25	0.428	0.6390	56.75	55.00	24.30	26.75	30 727	6.11	5374	21 534	3.20	122	2660	1.10
2.50	0.428	0.9914	55.30	54.10	25.50	28.15	31 719	5.89	5433	32 483	3.30	159	3447	1.00
2.50	0.405	1.1234	54.30	53.20	24.50	27.55	29 426	6.03	5142	36 263	3.36	195	4237	1.07
2.50	0.396	1.5020	52.20	51.30	25.20	28.40	29 319	5.91	5068	47 012	3.47	262	5657	1.20
$d_p = 191\ \mu m$, $\kappa = 0.423$, $D_e = 30$ mm, $A_{ii} = \pi(0.020)(1.22)\ m^2$, $A_{io} = \pi(0.022)(1.22)\ m^2$														
0.75	0.427	0.6390	56.45	54.70	24.20	26.70	30 603	6.12	5356	21 551	3.26	128	2773	1.13
0.75	0.427	0.9830	55.05	53.80	24.80	27.50	31 126	6.01	5375	32 692	3.33	161	3486	1.00
0.75	0.405	1.1234	54.55	53.45	24.90	27.85	29 694	5.96	5164	37 035	3.34	185	3999	1.00
0.75	0.395	1.5040	52.80	51.95	25.25	28.35	29 263	5.91	5062	47 922	3.42	228	4982	1.05
1.25	0.427	0.6310	55.70	54.00	23.80	26.20	30 265	6.20	5322	21 456	3.21	123	2648	1.09
1.25	0.427	0.9914	54.60	53.40	24.45	27.10	30 866	6.06	5360	32 477	3.35	157	3393	1.00
1.25	0.405	1.1234	54.35	53.30	25.10	27.85	29 763	5.95	5166	36 746	3.36	166	3583	1.00
1.25	0.395	1.4975	51.85	51.00	24.85	27.95	28 937	5.96	5033	47 190	3.50	244	5252	1.12
2.50	0.428	0.6390	52.35	50.85	23.25	25.35	29 840	6.31	5261	19 961	3.48	116	2498	1.11
2.50	0.427	0.9970	52.50	51.35	24.15	26.70	30 570	6.13	5313	31 304	3.46	180	3893	1.11
2.50	0.407	1.1234	53.70	52.60	24.95	27.80	29 855	5.96	5179	35 926	3.39	184	3999	1.00
2.50	0.392	1.4975	52.95	52.15	26.20	29.15	29 558	5.78	5074	47 346	3.45	216	4678	1.00

(*Continued overleaf.*)

Table 4. *Continued*

C_f [wt%]	$\dot{m}_w$ [kg s^{-1}]	$\dot{m}_s$ [kg s^{-1}]	T_{si} [°C]	T_{so} [°C]	T_{wi} [°C]	T_{wo} [°C]	Re_w	Pr_w	h_w [W m^{-2} K^{-1}]	Re_s	Pr_s	Nu_s	h_s [W m^{-2}K^{-1}]	h_s/h_{sw}
$d_p = 72$ μm, $\kappa = 0.538$, $D_e = 24$ mm, $A_{ii} = \pi(0.026)(1.22)$ m^2, $A_{io} = \pi(0.028)(1.22)$ m^2														
0.75	0.608	0.6310	48.75	46.75	19.00	21.00	29 424	7.09	4120	17 466	3.72	116	3100	1.40
0.75	0.634	0.9914	45.15	43.75	18.95	21.05	30 688	7.09	4225	25 762	4.00	176	4665	1.19
0.75	0.658	1.1280	43.35	42.15	18.55	20.50	31 423	7.19	4308	28 420	4.14	179	4723	1.07
0.75	0.686	1.4975	40.65	39.70	18.55	20.50	32 819	7.19	4436	36 095	4.35	253	6651	1.21
1.25	0.608	0.6310	49.00	46.90	18.95	21.05	29 431	7.09	4122	17 431	3.71	125	3359	1.52
1.25	0.634	0.9914	45.80	44.30	19.30	21.45	30 993	7.02	4245	25 926	3.95	181	4813	1.21
1.25	0.658	1.1280	44.30	43.05	19.25	21.30	32 050	7.04	4350	28 710	4.07	193	5132	1.18
1.25	0.686	1.4975	40.30	39.40	18.85	20.75	33 074	7.13	4446	35 719	4.38	255	6690	1.24
2.50	0.608	0.6310	46.40	44.30	18.05	20.10	28 737	7.29	4057	16 360	3.92	137	3666	1.86
2.50	0.634	0.9914	44.90	43.35	18.75	20.75	30 491	7.15	4212	25 146	4.03	160	4264	1.12
2.50	0.658	1.1280	42.90	41.70	18.75	20.70	31 615	7.15	4316	27 692	4.17	189	5021	1.18
2.50	0.686	1.4975	38.70	37.80	18.45	20.25	32 689	7.23	4412	34 336	4.51	261	6865	1.29
$d_p = 127$ μm, $\kappa = 0.538$, $D_e = 24$ mm, $A_{ii} = \pi(0.026)(1.22)$ m^2, $A_{io} = \pi(0.028)(1.22)$ m^2														
0.75	0.608	0.6310	48.10	46.00	18.30	20.40	28 960	7.23	4082	17 214	3.79	129	3447	1.55
0.75	0.634	0.9914	45.70	44.30	18.90	21.00	30 649	7.11	4228	26 013	3.96	167	4442	1.11
0.75	0.658	1.1280	43.40	42.20	18.60	20.55	31 489	7.18	4314	29 225	4.01	178	4723	1.02
0.75	0.686	1.4975	40.70	39.80	18.45	20.35	32 720	7.22	4428	36 095	4.35	232	6091	1.12
1.25	0.608	0.6310	48.20	46.30	18.70	20.65	29 206	7.15	4103	17 155	3.77	113	3016	1.40
1.25	0.634	0.9914	44.60	43.30	18.95	20.85	30 610	7.12	4215	25 378	4.05	149	3939	1.00
1.25	0.658	1.1280	43.20	42.00	18.05	20.05	31 084	7.25	4307	28 180	4.18	184	4842	1.11
1.25	0.686	1.4975	39.90	39.00	17.95	19.85	32 322	7.38	4379	35 514	4.41	244	6426	1.19
2.50	0.608	0.6310	43.15	41.60	18.25	19.75	28 663	7.30	4022	15 553	4.16	97	2583	1.48
2.50	0.634	0.9914	44.50	43.10	18.80	20.85	30 550	7.13	4211	25 017	4.05	175	4661	1.22
2.50	0.658	1.1280	43.30	42.10	18.80	20.70	31 632	7.15	4324	27 861	4.15	172	4559	1.06
2.50	0.686	1.4975	40.75	39.80	18.85	20.75	33 072	7.13	4450	35 521	4.34	240	6330	1.18
$d_p = 191$ μm, $\kappa = 0.538$, $D_e = 24$ mm, $A_{ii} = \pi(0.026)(1.22)$ m^2, $A_{io} = \pi(0.028)(1.22)$ m^2														
0.75	0.608	0.6310	47.85	45.75	18.35	20.50	29 014	7.28	4064	17 135	3.81	139	3709	1.71
0.75	0.634	0.9914	44.60	43.30	18.55	20.60	30 431	7.16	4207	25 500	4.05	170	4500	1.18
0.75	0.658	1.1280	43.00	41.80	18.65	20.55	31 518	7.17	4315	28 218	4.17	176	4636	1.07
0.75	0.686	1.4975	40.00	39.15	18.25	20.05	32 514	7.27	4414	35 727	4.40	215	5639	1.04
1.25	0.608	0.6310	45.00	43.20	18.45	20.25	28 960	7.29	4032	16 187	4.03	121	3220	1.70
1.25	0.634	0.9914	44.65	43.25	18.85	20.90	30 611	7.12	4216	25 385	4.04	174	4611	1.22
1.25	0.658	1.1280	43.00	41.75	18.30	20.35	31 295	7.24	4298	28 095	4.17	204	5397	1.26
1.25	0.686	1.4975	40.60	39.70	18.55	20.45	32 823	7.19	4437	35 877	4.35	236	6218	1.15
2.50	0.608	0.6310	43.45	41.75	18.75	20.40	29 185	7.16	4050	15 575	4.15	118	3123	1.83
2.50	0.634	0.9914	46.30	44.75	20.10	22.40	31 723	6.83	4304	25 860	3.91	216	5750	1.46
2.50	0.658	1.1280	45.70	44.30	20.05	22.35	29 271	7.68	4252	29 091	3.97	254	6776	1.51
2.50	0.686	1.4975	42.20	41.25	19.80	21.75	33 908	6.93	4512	36 459	4.22	236	6245	1.12

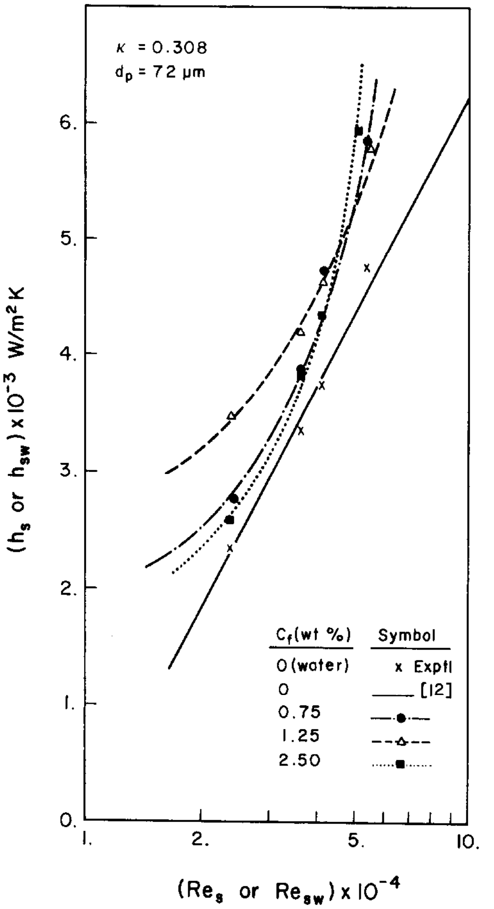

Fig. 3. Plot of h_s vs Re_s with C_f as a parameter for $\kappa = 0.308$ and $d_p = 72$ μm.

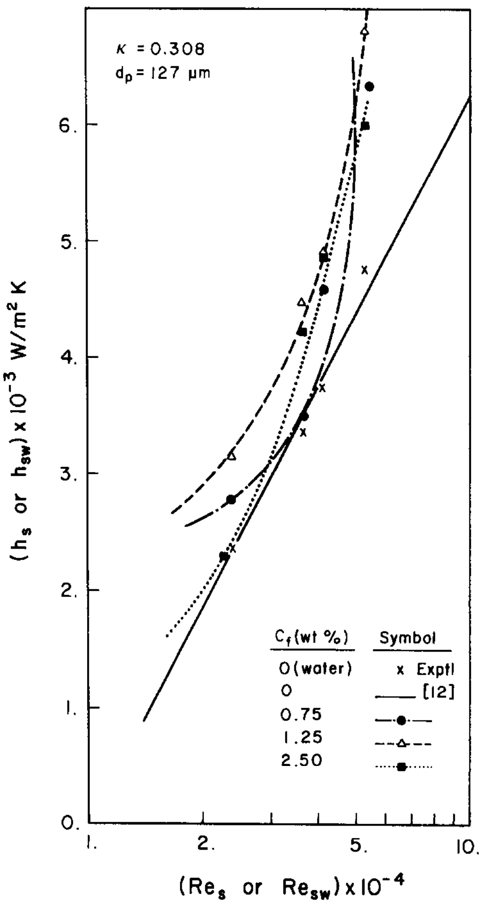

Fig. 4. Plot of h_s vs Re_s with C_f as a parameter for $\kappa = 0.308$ and $d_p = 127$ μm.

which caused shifts in these reference lines. The approximate ranges of Reynolds and Prandtl numbers for each aspect ratio are:

$Re_s = 23\,000$–$55\,000$; $Pr_s = 3.08$–3.40 for $\kappa = 0.308$

$Re_s = 21\,000$–$48\,500$; $Pr_s = 3.15$–3.50 for $\kappa = 0.423$

$Re_s = 17\,500$–$36\,000$; $Pr_s = 3.71$–4.50 for $\kappa = 0.538$.

The most important factors affecting the heat transfer mechanism in particulate flows were explained in the literature by Tien [16], Boothroyd [2], Depew [17] and Danziger [18] as boundary-layer thinning, wall-contact heat transfer and the reduced eddy diffusivity at the wall. Additionally, the importance of radial concentration distribution of solid particles on the heat transfer mechanism was emphasized by Furuta *et al.* [19] and Konno *et al.* [7]. Based on the information in the literature, the results of this study can be analysed as follows.

Figures 3–11 generally show that the slurry heat transfer coefficient increases with the Reynolds number, however almost every curve exhibits a minimum vertical distance to its reference line of 'h_{sw} vs Re_{sw}' at an intermediate Reynolds number indicating a minimum enhancement ratio (h_s/h_{sw}). In this range of the Reynolds number, h_s values may become even lower than h_{sw} values in some cases (see Figs. 6–8).

Increasing the Reynolds number to the intermediate values (e.g. 25 000–40 000) has a negative effect on the enhancement of heat transfer to or from liquid–solid flows due to the acquisition of high momentum by particles in the direction of flow, and prevention of their lateral motion, which contributes to the thinning of the viscous boundary layer. This effect is compensated by the increasing concentration of solids; therefore up to the intermediate Reynolds numbers, the heat transfer enhancement may decrease, but at higher Reynolds numbers the interaction between high-intensity eddies and the particles at high concentrations may create favourable patterns for better heat transfer.

Semilogarithmic plots of h_s vs Re_s in Figs. 6–8 and Figs. 10 and 11 show similar trends where the positive effects of low solid concentration at low Reynolds numbers (e.g. 15 000–20 000) and of high solid con-

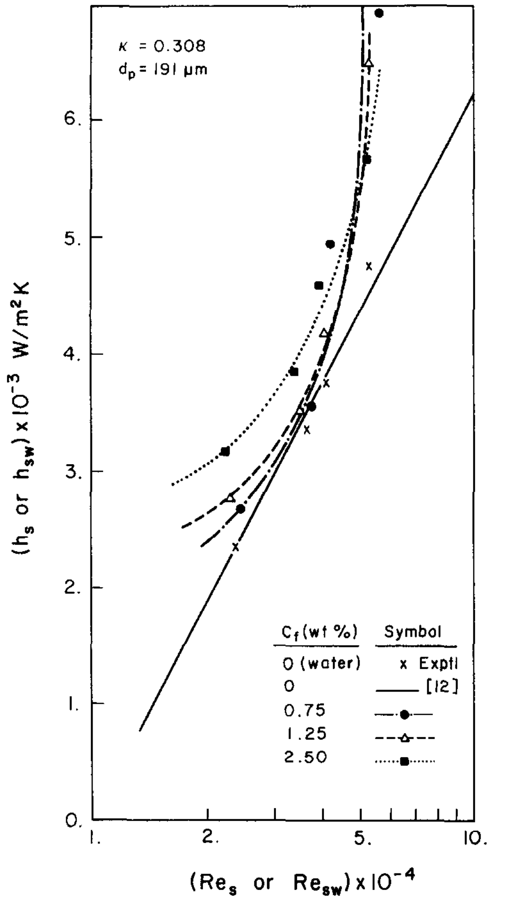

Fig. 5. Plot of h_s vs Re_s with C_f as a parameter for $\kappa = 0.308$ and $d_p = 191$ μm.

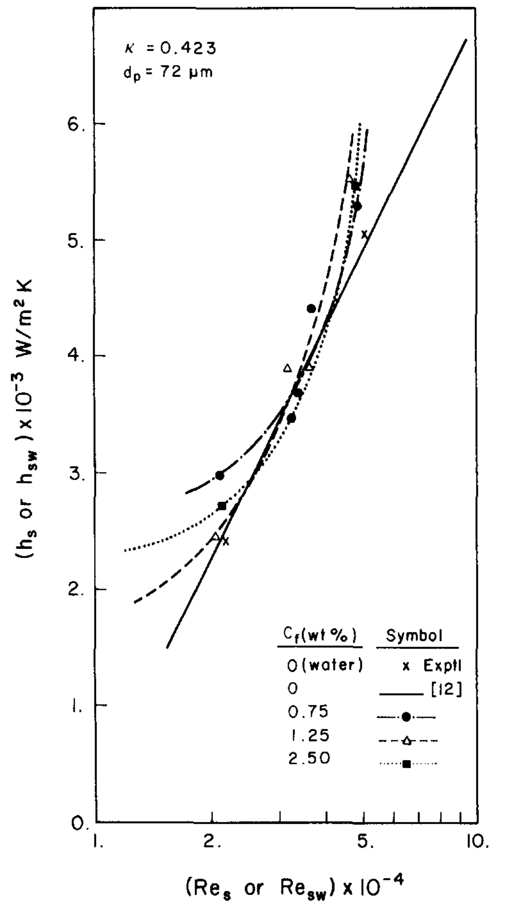

Fig. 6. Plot of h_s vs Re_s with C_f as a parameter for $\kappa = 0.423$ and $d_p = 72$ μm.

centration at high Reynolds numbers (e.g. 45 000–55 000) on heat transfer enhancement can be observed. The curves diverge from each other at low Reynolds numbers indicating that the increasing solid concentration is not beneficial to the heat transfer enhancement due to the limited freedom of particles in the lateral direction to thin the boundary layer and the increased effective viscosity of the suspension [2, 19]. The divergence of h_s vs Re_s curves from each other at low Reynolds numbers may be related to the magnitude of the agitation created by the particle–particle and the particle–wall interactions which in turn depend on the combined effects of particle size, width of annular gap, solid concentration, scale and intensity of turbulence. As the Reynolds number increases, although the effect of solid concentration on h_s is dominated by the effect of high turbulence, the favourable effect of high solid concentration (2.5 wt%) over those of other concentrations (0.75 and 1.25 wt%) can still be observed; because at high solid concentrations, wall-contact of the particles will be beneficial to the heat transfer mechanism only if the particle residence time at the wall is short and the particle–wall collision rate is large [2].

In Figs. 3–5 and 9 the beneficial effect of low solid concentration on h_s at low Reynolds numbers cannot be observed in water–feldspar flows through the largest annular gap ($D_e = 36$ mm) regardless of the particle size, or in those carrying the smallest particles ($d_p = 72$ μm) through the smallest annular gap ($D_e = 24$ mm). As can be observed in Figs. 3 and 4, the intermediate concentration (1.25 wt%) of small and medium size particles (72 and 127 μm) seems to provide a favourable flow behaviour for the heat transfer enhancement, which is reasonable, because in turbulent liquid–solid flows, the small particles will tend to follow the eddies and the two-phase mixture will behave roughly like a homogeneous liquid [2]. Therefore at low solid concentrations of small particles, particle–wall interactions will not be significant. As the solid concentration increases, the increased effective viscosity of homogeneous water–feldspar mixture will reduce the heat transfer rate; however, the intermediate concentrations of small particles may create particle–wall interactions [20] at a high level to enhance the rate of heat transfer (Figs. 3 and 4).

In Figs. 5 and 9, it seems that the behaviour of the largest particles (191 μm) in the largest annular gap ($D_e = 36$ mm) is similar to that of the smallest par-

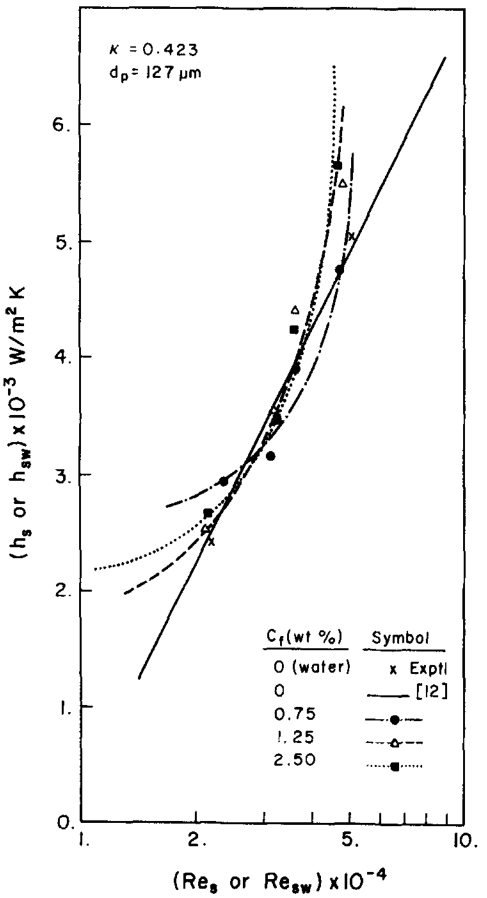

Fig. 7. Plot of h_s vs Re_s with C_f as a parameter for $\kappa = 0.423$ and $d_p = 127$ μm.

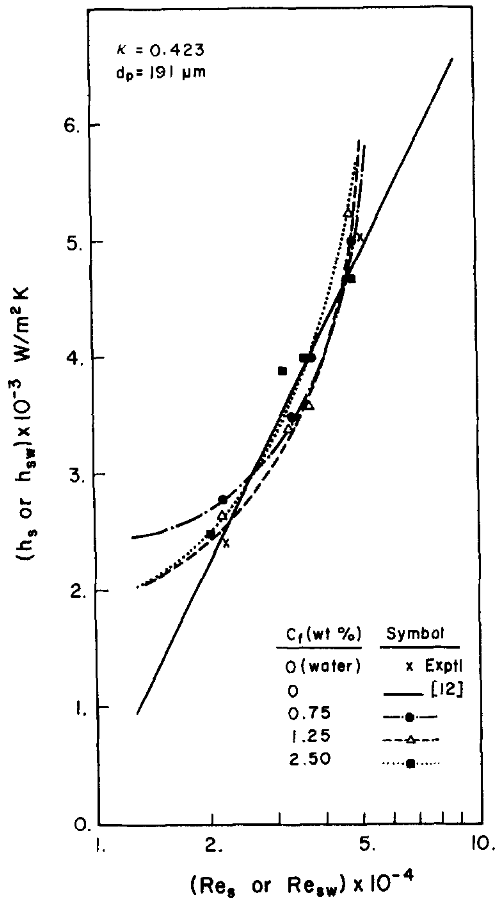

Fig. 8. Plot of h_s vs Re_s with C_f as a parameter for $\kappa = 0.423$ and $d_p = 191$ μm.

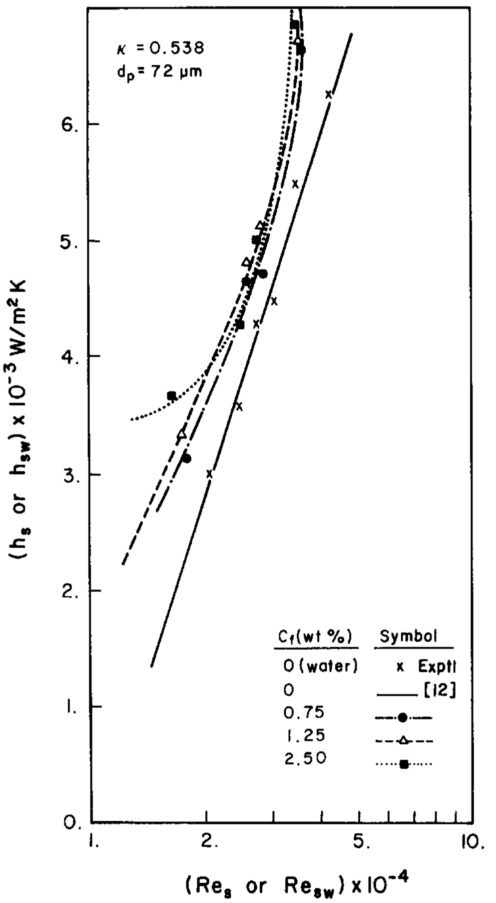

Fig. 9. Plot of h_s vs Re_s with C_f as a parameter for $\kappa = 0.538$ and $d_p = 72$ μm.

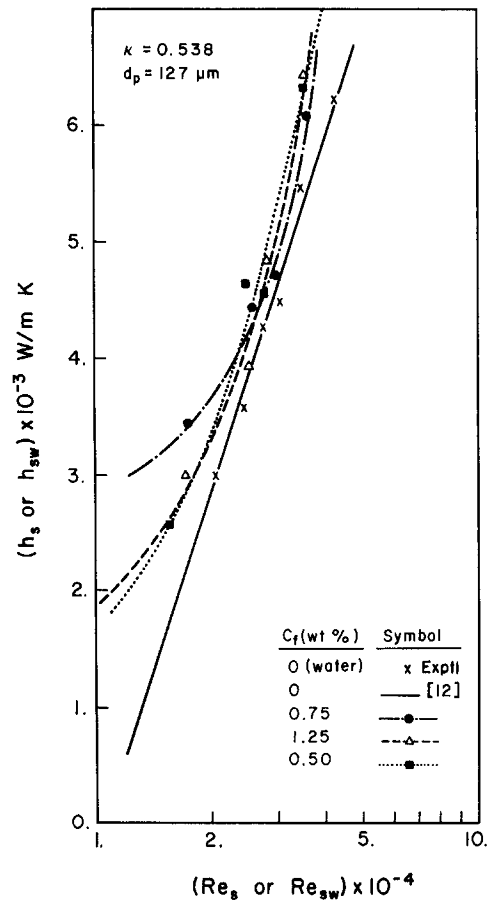

Fig. 10. Plot of h_s vs Re_s with C_f as a parameter for $\kappa = 0.538$ and $d_p = 127$ μm.

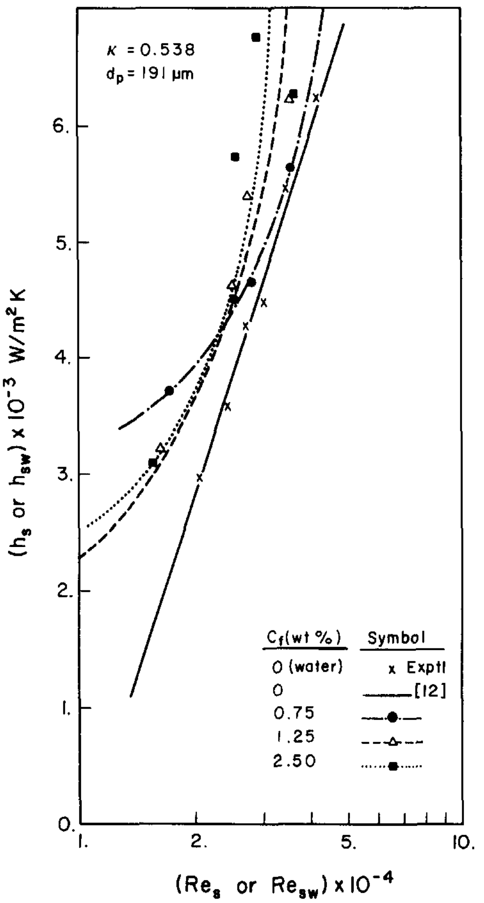

Fig. 11. Plot of h_s vs Re_s with C_f as a parameter for $\kappa = 0.538$ and $d_p = 191$ μm.

ticles (72 μm) in the smallest annular gap ($D_e = 24$ mm). In both of these cases, 2.5 wt% solid concentration yields higher heat transfer coefficients, h_s, and higher enhancement ratios (h_s/h_w) than those given by the other concentrations (0.75 and 1.25 wt%) at low Reynolds numbers. This can be explained again by the combined effects of particle–wall, particle–eddy interactions represented roughly by the D_e/d_p ratio and the solid concentration.

CONCLUSION

It is clear that the dependence of heat transfer enhancement on the experimental parameters is quite complex. The combined effects of particle size, width of annular gap, D_e/d_p ratio, solid concentration in the slurry, Prandtl and flow Reynolds numbers determine the percentage enhancement in heat transfer to or from the turbulent water–feldspar upflows through vertical annuli. In order to give more comprehensive explanations for the mechanism of enhancement in heat transfer, additional experimental data is needed.

REFERENCES

1. D. C. Schlüderberg, Gas suspension coolants for large nuclear reactors, *Part 1 of First Day Proceedings of Conference on Dust Cooling*, Queen Mary College, London (1964).
2. R. G. Boothroyd, *Flowing Gas–Solids Suspensions* (1st Edn), Chap. 7. Chapman & Hall, London (1971).
3. V. J. Kofanov, Heat transfer and hydraulic resistance in flowing liquid suspension in pipes, *Int. Chem. Engng* **4,** 426–430 (1964).
4. J. J. Salamone and M. Newman, Water suspensions of solids, *Ind. Engng Chem.* **47,** 283–288 (1955).
5. C. A. Brandon and D. G. Thomas, Transport characteristics of suspensions, *Proceedings of the Fourth International Heat Transfer Conference*, Paper CT-2.1, Paris (1970).
6. L. Plass and O. Molerus, Simultane wärmeübergangs- und druck verlustmessungen an feststoff/flüssigkeits-suspensionen im übergangsbereich vom homogenen zum heterogenen suspensions-transport, *Chemie-Ingr-Tech.* **46,** 355–356 (1974).
7. H. Konno, E. Harada, M. Toda, M. Kuriyama and S. Saruta, Heat transfer characteristics of solid–liquid upward flow through vertical pipes, *Kagaku Kogaku Ronbunshu* **6,** 308–311 (1980).
8. T. A. Özbelge, The location of peak heat transfer enhancement in suspension flows, *Int. J. Multiphase Flow* **19,** 535–538 (1993).
9. E. Harada, M. Toda, M. Kuriyama and H. Konno, Heat transfer between wall and solid–water suspension flow in horizontal pipes, *J. Chem. Engng Japan* **18,** 33–38 (1985).
10. C. J. Park, K. O. Choj and D. S. Doh, An experimental and theoretical study on the augmentation of heat transfer by suspended solid particles in the flowing fluid in a vertical tube, *Hwahak Konghak* **27,** 682–688 (1989).
11. R. Zisselmar and O. Molerus, Investigation of solid–liquid pipe flow with regard to turbulent modification, *Chem. Engng J.* **18,** 233–239 (1979).
12. B. S. Petukhov and L. I. Roizen, Generalized relationship for heat transfer in a turbulent flow of gas in tubes of annular section, *High Temp.* **2,** 65–68 (1964).
13. S. H. Köker Heat transfer characteristics of liquid–solid suspensions flowing turbulently upward in a vertical concentric annulus, M.Sc. thesis, Middle East Technical University, Ankara (1993).
14. E. N. Sieder and G. E. Tate, Heat transfer and pressure drop of liquids in tubes, *Ind. Engng Chem.* **28,** 1429–1435 (1936).
15. J. W. Smith and J. C. Paradi, Heat transfer to settling slurries in vertical transport, *J. Pipelines* **3,** 43–52 (1982).
16. C. L. Tien, Heat transfer by a turbulently flowing fluid–solids mixture in a pipe, *J. Heat Transfer (Trans. ASME) C* **83,** 183–188 (1961).
17. C. A. Depew, Heat transfer to flowing gas–solids mixtures in a vertical circular duct, Ph.D. thesis, University of California, Berkeley, CA (1960).
18. W. J. Danziger, Heat transfer to fluidized gas–solids mixtures in vertical transport, *Ind. Engng Chem. Process Design Dev.* **2,** 269–276 (1963).
19. T. Furuta, S. Tsujimoto, M. Okazaki and R. Toei, Concentration distribution of particles in solid–liquid two-phase flow through vertical pipe, *Kagaku Kogaku Ronbunshu* **4,** 605–615 (1978).
20. T. A. Özbelge and T. G. Somer, Hydrodynamic and heat transfer characteristics of liquid–solid suspensions in horizontal turbulent pipe flow, *Chem. Engng J.* **38,** 111–122 (1988).